Parameter Sensitivities Affecting the Flutter Speed of a MW-Sized Blade

Don W. Lobitz

Sandia National Laboratories,[1] P. O. Box 5800,
MS0708, Albuquerque, NM 87185-0708
e-mail: dwlobit@sandia.gov

With the current trend toward larger and larger horizontal axis wind turbines, classical flutter is becoming a more critical issue. Recent studies have indicated that for a single blade turning in still air the flutter speed for a modern 35 m blade occurs at approximately twice its operating speed (2 per rev), whereas for smaller blades (5–9 m), both modern and early designs, the flutter speeds are in the range of 3.5–6 per rev. Scaling studies demonstrate that the per rev flutter speed should not change with scale. Thus, design requirements that change with increasing blade size are producing the concurrent reduction in per rev flutter speeds. In comparison with an early small blade design (5 m blade), flutter computations indicate that the non rotating modes which combine to create the flutter mode change as the blade becomes larger (i.e., for the larger blade the second flapwise mode, as opposed to the first flapwise mode for the smaller blade, combines with the first torsional mode to produce the flutter mode). For the more modern smaller blade design (9 m blade), results show that the non rotating modes that couple are similar to those of the larger blade. For the wings of fixed-wing aircraft, it is common knowledge that judicious selection of certain design parameters can increase the airspeed associated with the onset of flutter. Two parameters, the chordwise location of the center of mass and the ratio of the flapwise natural frequency to the torsional natural frequency, are especially significant. In this paper studies are performed to determine the sensitivity of the per rev flutter speed to these parameters for a 35 m wind turbine blade. Additional studies are performed to determine which structural characteristics of the blade are most significant in explaining the previously mentioned per rev flutter speed differences. As a point of interest, flutter results are also reported for two recently designed 9 m twist/coupled blades. [DOI: 10.1115/1.2037091]

Keywords: Classical Flutter, Flutter Parameter Sensitivity, Wind Turbine Blade

1 Introduction

Early and recent investigations of stability in wind turbine blades address the issue of classical flutter for smaller rotors (~10 m blades) [1–3]. These simulations, which apply linear aerodynamics to a blade turning in still air, indicate flutter rotational speeds of the order of 5 times the operating speed of the rotor. The mode shape associated with the onset of flutter generally consists of a coupling of the second flapwise and first torsional modes of the stationary blade. In the recent past classical flutter investigations have also been completed for larger blades (~35 m blades) [4,5]. Results from these simulations indicate flutter rotational speeds in the realm of two times the operational speed of the rotor. As with the smaller rotors the flutter mode shape also consists of a coupling of the second flapwise and first torsional modes.

Simple scaling of the dimensions of the blade, without altering the materials of which it is made, indicate that the per rev flutter speed (ratio of the flutter rotational speed to the rotor operating speed) should not change with scale, nor should the character of the flutter. This observation is primarily motivated by the nondimensional form of the classical flutter solution for an infinitely long airfoil [6], on which the simulations presented here are based. For the more structurally complex blades addressed in this

work, this independence of scale still holds, as will be demonstrated. As nondimensional forms are not plausible for these complex blades, a modern larger blade can be scaled down to the size of a modern smaller one so that one-to-one comparisons of the two blades can be made. Using this comparison as a guide, parameters for the scaled larger blade can be artificially altered through simulation in an attempt to identify the critical parameters that lead to the noted marked reduction in the per rev flutter rotational speed.

A number of the important critical parameters are identified in text books [7–9]. These texts have also recommended parameter variances to minimize the prospect of flutter, as outlined below:

- Move the chordwise center of mass (inertia axis) forward. When the center of mass is ahead of the shear center of the wing, flutter is unlikely at any speed.
- Increase the torsional natural frequency of the blade by increasing its torsional stiffness.
- Maximize the ratio of the torsional to flapwise natural frequencies of the modes that combine to produce the flutter mode.
- Move the elastic and inertia axes toward the line of aerodynamic centers (1/4 chord).
- Decrease the blade aspect ratio (span/average chord).
- Decrease the air-to-blade mass ratio (ratio of the mass per unit length of the air in a circular cross section with the chord as its diameter to the mass per unit length of the blade).

Through simulation, this paper attempts to identify design changes that develop as a result of increasing blade size that may

---

lead to significantly lower per rev flutter speeds. In the course of this analysis flutter speed sensitivities to various design parameters are developed which can assist the designer in raising the per rev flutter speed of a given blade.

The simulations in this work are based on single blade analysis in order to expedite a process that requires multiple solutions for investigating a number of parameter spaces. As such, the analysis may be unconservative as the modes of a complete wind turbine contain significant blade-to-blade and blade-to-tower interactions. The analysis may also be unconservative as a result of the restrictive unsteady aerodynaminc model that is employed, as discussed in the following section. A more quantitative approach would combine a more complete unsteady aerodynamics model with a complete wind turbine model. However, the simple aeroelastic stability analyses presented here can still serve to identify flutter speed sensitivities to various design parameters.

The next section of the paper briefly outlines the technique used for the prediction of classical flutter speeds, physical comparisons between the scaled-large and small blades, and classical flutter details for each blade. Following this, results of the investigation into the possible causes of the flutter speed reductions that seem to occur as the blade size increases are provided. Lastly, a summary with conclusions is presented.

2 Methods and Models

Focusing on aeroelastic stability associated with the shed wake, the frequency-domain technique developed by Theodorsen [6–10] for predicting classical flutter in fixed wing aircraft has been adapted for use with a rotor blade. This method assumes that the flow always remains attached and in the linear aerodynamic regime. Additionally, as long as these conditions are met, steady angles of attack are not particularly relevant to the classical flutter phenomenon. The prediction of classical flutter is based more on oscillations about these steady angles of attack. Thus, to simplify the analysis the rotor is assumed to be turning in still air, and, for no inflow, unsteady aerodynamics caused by the trailing wake can be neglected. Consequently, the aerodynamics for a single blade is similar to that of a fixed wing with a free stream velocity that varies linearly from the root to the tip, assuming that the shed wake of the preceding blade dies out sufficiently fast so that the oncoming blade will encounter essentially still air. The blade also differs from the wing structurally in that it is centrifugally stiffened and rotating coordinate system effects are included in the equations of motion (i.e., Coriolis and centrifugal softening terms). Aerodynamic quantities that vary along the span of the blade, such as the semi-chord, b, the free stream velocity, U, and the lift curve slope, are included using a finite element technique wherein the quantities are assumed to vary linearly over the length of the element and are then included within the integral over the element length associated with the principle of virtual work used in the development of the element. The structural properties of the blades are modeled with NASTRAN [11] tapered beam (CBEAM) elements, which have six degrees of freedom at either end. These elements have provision for shear deformation and warping of the cross section, although these features were not used in this analysis.

Theodorsen's solution is couched in the frequency domain and contains both circulatory and noncirculatory aerodynamic terms. These terms are linear functions of the blade angle of attack, its first and second time derivatives, and the first and second time derivatives of the blade plunging motion (flapping motion perpendicular to the free stream). Moreover, the circulatory terms are multiplied by a complex-valued function (the Theodorsen function) which depends on the reduced frequency and, hence, the frequency of the flutter oscillation. The presence of this function necessitates an iterative solution procedure since the flutter oscillation frequency is not known a priori. It might be noted here that a state-space formulation of Theodorsen's unsteady aerodynamics exists, employing a two-term exponential approximation to the
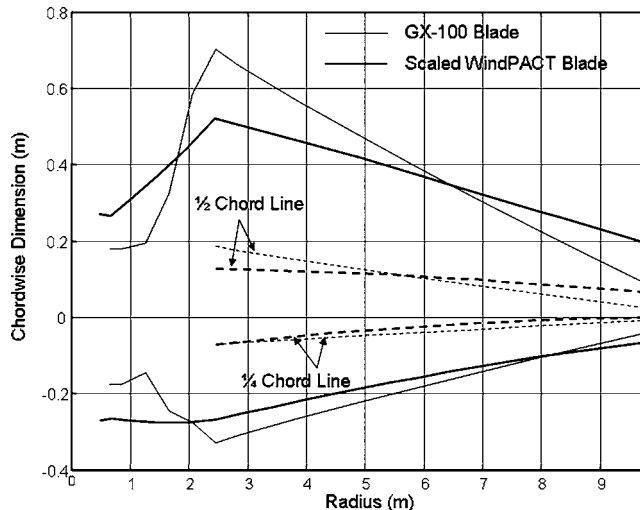
Theodorsen function wherein the need for iteration is eliminated [5]. Although superior, this technique has not been used for the present work due to the resource constraints associated with acquisition of such a software tool. Additional details of the procedure and general technique used here for predicting classical flutter in wind turbine blades can be found in [4].

The blades selected for this study have both been designed in the recent past employing modern design practices associated with the use of glass-fiber-reinforced plastics. The larger blade is the WindPACT blade [12], which has a blade length of 33.35 m. With a tip radius of 35 m, it is designed to operate on a three-bladed 1.5 MW rotor having a maximum rotor speed of 20.5 rpm (0.342 Hz). The smaller blade is the GX-100 blade [2], which has a blade length of 9.2 m. It is designed to operate on a three-bladed 115 kW rotor with a tip radius of 9.86 m. For purposes of comparison to the larger rotor, this rotor is assumed to operate at an equivalent tip speed ratio, resulting in a maximum rotor speed of 72.8 rpm (1.213 Hz).

After scaling the larger blade down to the size of the smaller blade using a scale factor of 9.86/35.0, the superimposed planforms of the two blades are shown in Fig. 1. The bold curves depict the scaled WindPACT blade and the light ones, the GX-3100 blade (This will be the case in Figs. 1–5). The dashed lines
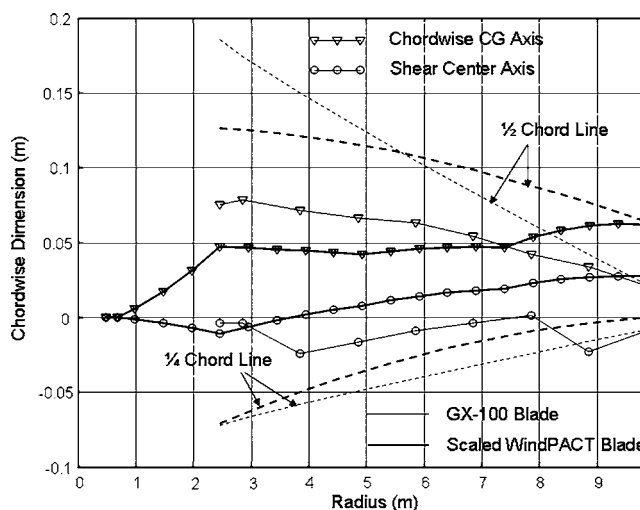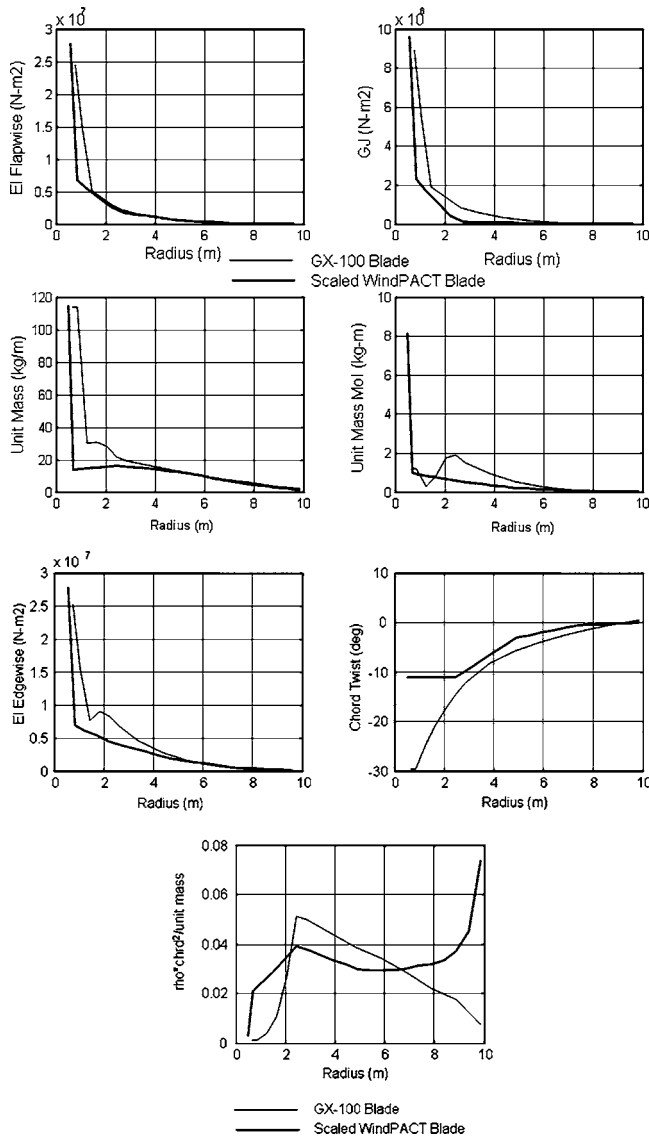

Fig. 1 Planforms of the scaled WindPACT and GX-100 blades

Fig. 2 Chordwise CG and shear center axis locations for the scaled WindPACT and GX-100 blades

Fig. 3 Structural and mass properties for the scaled Wind-PACT and GX-100 blades

Fig. 4 Second flapwise and first torsional stationary (non rotating) mode shapes for the scaled WindPACT and GX-100 blades

rigidity (EIf), the unit mass (mass per unit length), the torsional rigidity (GJ), the unit mass moment of inertia (mass moment of inertia per unit length), the edgewise flexural rigidity (EIe), and the chordwise twist distribution are shown as a function of span. Some of these properties are critical because they govern the flapwise and torsional natural frequencies of the blade, which strongly influence the onset of classical flutter. The flapwise flexural rigidity and unit mass curves track well beyond a radius of 4 m, but deviate inboard of that point. The torsional rigidity and unit mass moment of inertia curves display significant deviations over a larger region of the blade span than those of the flapwise flexural rigidity and unit mass, with the GX-100 blade exhibiting greater values for both the torsional rigidity and the unit mass moment of inertia. The dip in the unit mass moment of inertia between the radii of 1 and 2 m for the GX-100 blade is the result of a thinning of the skin while preserving the outside diameter in that region. The edgewise flexural rigidity variations mimic those of the torsional rigidity except for a dip in the GX-100 curve similar to that of its unit mass moment of inertia curve. Generally the chordwise twist for the GX-100 blade is greater than that for the WindPACT blade, with significant deviations occurring inboard of 2.5 m. Also shown in Fig. 3 is a comparison of the air-to-blade mass ratio (or a measure thereof, $\text{rho} \times \text{chrd}^2/\text{blade mass per unit length}$) for the

denote the $\frac{1}{4}$ and $\frac{1}{2}$ chord lines for each blade. The chord averages are nearly equal with the scaled WindPACT blade at 0.5438 m and the GX-100 blade at 0.5610 m, yielding similar aspect ratios of 18.13 and 17.58 respectively. However, the blade tapers are significantly different, producing an added degree of "stubbiness" for the GX-100 blade (a quality also apparent in blades having lower aspect ratios).
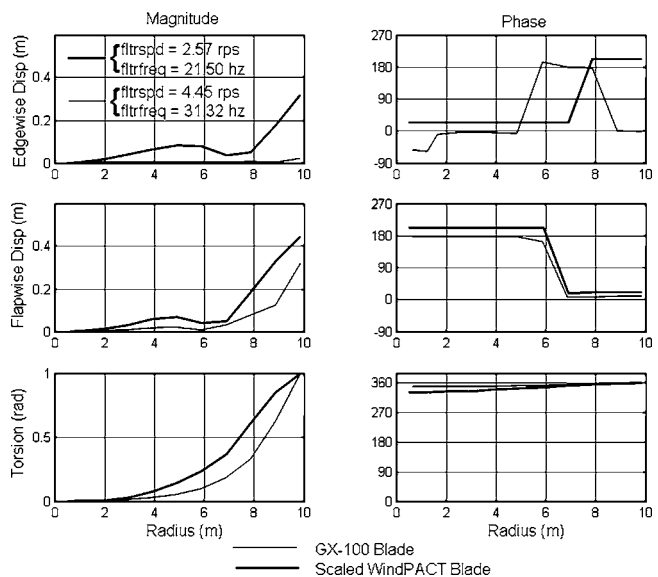
Figure 2 provides a zoom-in of Fig. 1 showing additional information in the region between the $\frac{1}{4}$ and $\frac{1}{2}$ chord lines for each blade. As mentioned above, the bold curves depict the scaled WindPACT blade and the light ones, the GX-100 blade. The curves with the inverted triangles denote the chordwise center of mass axes, and the ones with the circles, the shear center axes. Note that for the GX-100 blade, the center of mass axis is generally further aft of the shear center axis than that of the scaled WindPACT blade. Also for the GX-100 blade, the shear center axis appears on average to be closer to the $\frac{1}{4}$ chord line, i.e., further forward than that of the WindPACT blade.

In Fig. 3 a comparison of critical distributed beam and mass properties for the two blades is presented. For this comparison, the properties of the WindPACT blade are scaled linearly using the scale factor given above. Comparisons of the flapwise flexural

Fig. 5 Classical flutter complex-mode shapes for the scaled WindPACT and GX-100 blades

Table 1 Flutter results for the full and scaled WindPACT blades (scale factor =9.86/35=0.2817)

Quanity	Full-Size WindPACT blade	Scaled WindPACT blade
Flutter frequency (Hz)	6.057	21.50
Flutter speed (rps)	0.723	2.566
Operating speed (rps)	0.342	1.213
Per rev flutter speed	2.114	2.115

Fig. 6 Per rev flutter speed variation with frequency ratio for the WinPACT blade

two blades. The dramatic difference near the tip is primarily caused by the relatively larger chord of the scaled WindPACT blade in that region.

The mode shapes of the stationary blades (not rotating) that couple in flutter are shown in Fig. 4. They consist of the second flapwise mode and the first torsional mode. For the GX-100 blade the second flapwise mode seems to exhibit greater activity near the tip than that of the scaled WindPACT blade. The natural frequencies are markedly different, leading to significantly different torsional to flapwise frequency ratios; 45.25/8.50=5.32 for the GX-100 blade and 31.27/12.77=2.45 for the scaled WindPACT blade.

3 Results

Figure 5 shows a comparison of the flutter modes for the two blades. These modes are complex strictly due to the effects of the aeroelasticity, as damping has not been included in these analyses. In the flapwise direction the motion is consistent with the second flapwise mode behavior. Note the significant edgewise motion in the flutter mode for the scaled WindPACT blade. Due to blade design differences, the flutter speed for the scaled WindPact blade is significantly down from that of the GX-100 blade; 2.57 rps vs. 4.45 rps, respectively. The flutter frequency of the scaled Wind-PACT blade is also significantly down from that of the GX-100 blade (21.50 Hz vs. 31.32 Hz, respectively). But, as expected, both are down from their respective torsional natural frequencies shown in Fig. 4.

It is of interest to note that the flutter speed for the scaled WindPACT blade scales perfectly from the parent full-scale Wind-Pact blade, as indicated in Table 1. As shown, the flutter frequency also scales perfectly. The flutter mode shapes are slightly different in that the dominant motion for the full-scale blade was the flapwise displacement rather than the torsional rotation Entirely similar behavior was noted when scaling the GX-100 blade up to the size of the WindPACT blade.

Reviewing the list in the Introduction that identifies parameter variances for minimizing the prospect of flutter, the two parameters that have significant potential for explaining the flutter speed difference for the two blades are the torsional stiffness for raising the torsional natural frequency, and the ratio of the torsional to flapwise natural frequencies. These two parameters are related, but can also be independent, and will be investigated below. As the aspect ratios of the two blades are close in value, this parameter is deemed not to be of much use in this study. The average air-to-blade mass ratios computed from the distributions shown in Fig. 3 are 0.0279 for the GX-100 blade and 0.0327 for the scaled WindPACT blade, an increase of 17%. When this parameter for the scaled WindPACT blade is reduced to that of the GX-100 blade through either air density or chord reductions, only small increases in the per rev flutter speed are noted (less than 5%). Since the chordwise center of mass axis for the GX-100 blade is more aft of its corresponding shear center axis than that of the scaled WindPACT blade (and therefore likely to be less stable), this parameter will probably not be of use in explaining the greater per rev flutter speed GX-100 blade. To verify this, however, results will be presented that show how this parameter affects flutter speed for the WinPACT blade. Lastly, selected blade properties of the WindPact blade will be systematically replaced
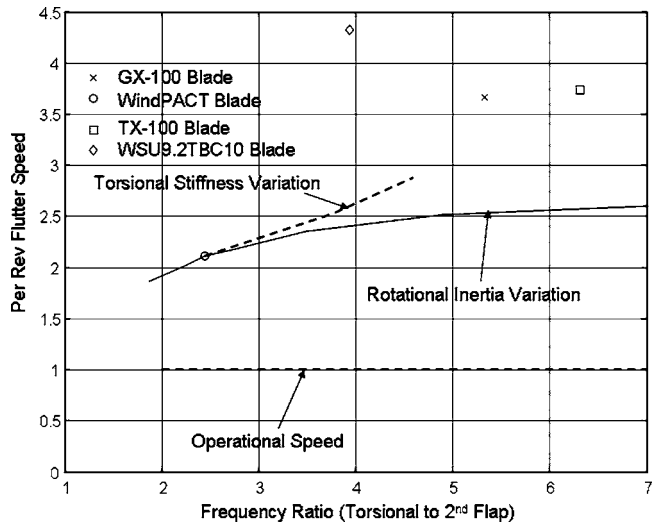
by scaled up properties of the GX-100 blade to determine which ones, individually and/or in combination, are of most importance in raising the flutter speed of the WindPACT blade to that of the GX-100 blade.

For modifying the two promising parameters discussed above, two approaches were used. The first was to incrementally modify the torsional stiffness of the WindPACT blade from its design stiffness to a scaled stiffness equivalent to that of the GX-100 blade. This produces an increase in the torsional stiffness of the WindPACT blade. As all other blade properties remain unchanged, this alteration produces an increased torsional frequency and an increased torsional to second flapwise frequency ratio, both of which should cause the per rev flutter speed to increase. In the second approach the rotational inertia of the WindPACT blade was modified by symmetrically moving the blade mass fore and aft about the mass center to alter the torsional frequency of the blade. When the blade mass is represented by two equal mass distributions placed equidistant fore and aft of the center of mass, the juxtaposition of the two distributions ranges from 40 to 60% of the blade chord to obtain accurate design values of the blade rotational moment of inertia along the blade span. To affect the changes in the mass moment of inertia, this distance between the mass distributions was incrementally varied between 10 and 120% of these baseline values. As before all other blade properties remain unchanged with this alteration. When the rotational inertia is decreased the torsional frequency increases leading to an increase in the torsional to second flapwise frequency ratio and an associated increase in the per rev flutter speed. Although specific results are not presented here, these modifications also affect the mode shapes of the blades and in particular the phasing between them, which is known to be important in classical flutter.

Results from these modifications are shown in Fig. 6 where the per rev flutter speed is plotted versus the non rotating torsional to second flap frequency ratio. The operational rotor speed is denoted by the horizontal dashed line at 1 per rev. The circle denotes per rev flutter data for the unaltered WindPACT blade and the "x," the GX-100 blade. The dashed curve in Fig. 6 labeled "Torsional Stiffness Variation" tracks the per rev flutter speed of the Wind-PACT blade as its torsional stiffness is incrementally increased to a scaled stiffness equivalent to that of the GX-100 blade at the right-most end of the curve. Although the per rev flutter speed significantly increases, by itself the torsional stiffness variation is not enough to close the gap in per rev flutter speed between the WindPact blade and the GX-100 blade. Likewise, as indicated by the curve labeled "Rotational Inertia Variation," when the fre-
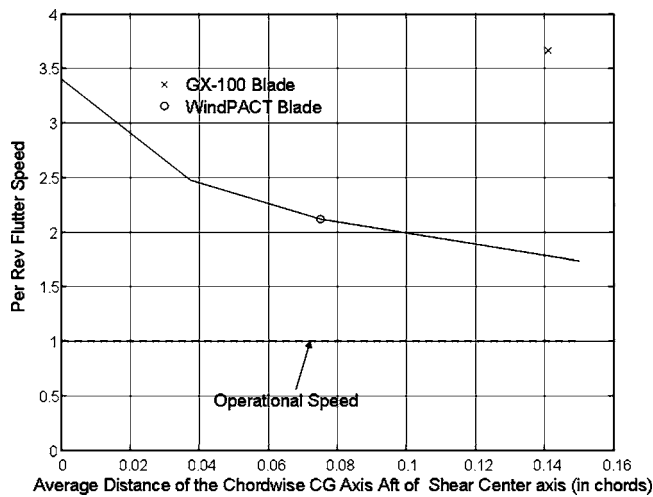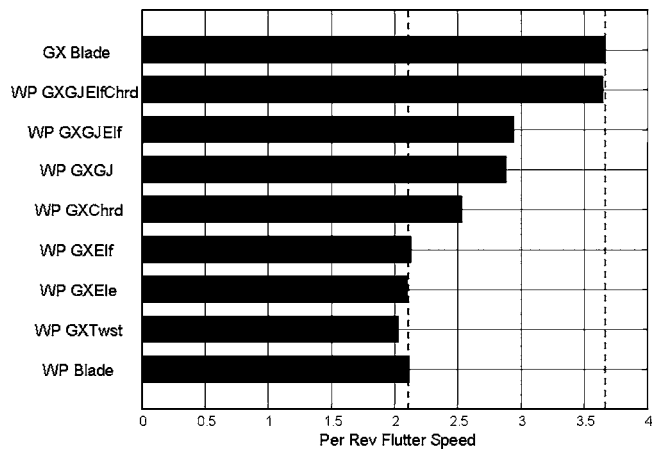
Fig. 7 Per rev flutter speed variation with average chordwise CG and shear center axis separation

Fig. 8 WindPACT flutter speed variations resulting from the selective substitution of scaled GX-100 properties

quency ratio of the WindPACT blade is increased by decreasing the rotational inertia, the more modest increases in per rev flutter speed are not sufficient to close the gap.

Ideally, to show ramifications of design trends in moving from smaller to larger blade designs, flutter predictions for a number of smaller and larger blade designs are desirable. Unfortunately, details on many of the blade designs are unavailable primarily because they are proprietary. However, as indicated in Fig. 6, details for two additional smaller blade designs are available, represented by the square and the diamond corresponding to flutter data for the TX-100[2] and the WSU9.2TBC10[3] blades, respectively. These blades are in the smaller blade category (~9 m) and are designed using a carbon-glass hybrid layup that twists as it bends [13]. They also exhibit higher per rev flutter speeds similar to that of the GX-100 blade. A possible explanation for the especially high flutter speed of the WSU9.2TBC10 blade in conjunction with a lower frequency ratio is that in that blade the chordwise center of mass axis is assumed to lie on the shear center axis. This tends to elevate the flutter speed relative to cases where that axis lies aft of the shear center axis (the usual case for the other blades investigated here).

To verify that the position of the chordwise center of mass axis relative to the shear center axis will not be of use in explaining the greater per rev flutter speed of the GX-100 blade, results are presented in Fig. 7 that show how this parameter affects flutter speed for the WinPACT blade. In this figure the abscissa represents the average distance in chords that the Chordwise CG axis is aft of the shear center axis. When the distance is zero, they are collinear. As before, the circle indicates the per rev flutter data for the unaltered WindPACT blade, and the "x," the GX-100 blade. As the location of the CG axis of the WindPACT blade is modified to more closely replicate that of the GX-100 blade, the gap in the per rev flutter speeds widens, as expected.

In Fig. 8 WindPACT blade properties are systematically altered, individually and/or in combinations, to provide explanations for the noted flutter speed differences. Blade properties that affect the various classes of mode shapes (flapwise, edgewise, and torsional) are modified so as to be scaled replicas of those of the GX-100 blade. Blade twist and chord distributions are also replaced by scaled versions of those of the GX-100 blade. Finally, combinations of these modifications are explored to fully understand the design differences between these two blades that lead to the significant differences in per rev flutter speed. The lowest bar in Fig. 8 corresponds to the per rev flutter speed of the unaltered Wind-PACT blade, and the highest one, that of the GX-100 blade. The vertical dashed lines help to gauge where modified WindPACT

configurations fall between these two flutter speeds. As indicated in Fig. 8, the individual substitution of the GX-100 twist distribution and edgewise flexural rigidity (EIe) both produce a reduction in the WindPACT blade's flutter speed, whereas the individual substitution of the flapwise flexural rigidity (EIf), the torsional rigidity (GJ), and the chord distribution all produce an increase in flutter speed (the torsional rigidity and chord distribution producing much more significant increases than the flapwise flexural rigidity). In combining the flapwise flexural and torsional rigidities (GJEIf) a slight synergistic effect is noted in that the combination produces a result that is a little larger that the sum of the individual contributions. An even greater synergistic effect occurs when these two scaled GX-100 rigidities are combined with the scaled GX-100 chord distribution (GJEIfChrd), producing a per rev flutter speed nearly equal to that of the GX-100 blade. Replacing all WindPACT blade properties with scaled GX-100 ones is equivalent to scaling the GX-100 blade up to the WindPACT blade size, and, as noted previously, since the flutter speed scales perfectly, the GX-100 per rev flutter speed is attained.

4 Summary and Conclusions

Clearly, from the discussion above, modification of the critical parameters that affect the per rev flutter speed cannot account for the difference between the per rev flutter speeds of the scaled WindPACT and GX-100 blades. Of the parameters investigated, increasing the torsional to second flap frequency ratio by increasing the torsional stiffness of the WindPACT blade provides the greatest increase in per rev flutter speed for closing the flutter speed gap (~50% closure). Increasing the frequency ratio by decreasing the rotational inertia of the WindPACT blade produces lesser increases in per rev flutter speed and is therefore less effective in closing the gap. Moving the Chordwise CG axis of the WindPACT blade further aft relative to the shear center axis to more closely replicate that of the GX-100 blade reduces the per rev flutter speed, increasing the per rev flutter speed gap. It is noted that in modifying these parameters, mode shapes and their relative phases, which play a crucial part in the classical flutter phenomenon, also change.

Systematically altering WindPACT blade properties individually and/or in combinations provides a better explanation for the noted flutter speed differences. Blade properties that affect the classes of mode shapes (flapwise, edgewise, and torsional) are modified to be scaled replicas of those of the GX-100 blade to determine per rev flutter speed sensitivity. Sensitivities are also determined for scaled versions of the GX-100 blade's twist and chord distributions. Finally, combinations of these modifications are explored to identify design differences between these to blades that lead to the significant differences in per rev flutter speed.

Results indicate that of the blade properties investigated the greater torsional rigidity and the more tapered chord distribution of the GX-100 blade primarily lead to its higher per rev flutter speed. Although significant individually, the combination of these two properties provides a substantial synergistic effect, enough to nearly close the gap between the unaltered WindPACT and the GX-100 per rev flutter speeds. The scaled replica of the flapwise flexural rigidity of the GX-100 blade turns out to be a minor contributor to its higher per rev flutter speed.

Studies such as this one (and hopefully more to follow) provide the blade designer with useful options for designing blades that are less likely to exhibit classical flutter. This may be especially important if, as this study indicates, the per rev flutter speed indeed tends to decrease with increasing blade size.

References

[1] Lobitz, D. W., and Veers, P. S., 1998, "Aeroelastic Behavior of Twist-Coupled HAWT Blades," *Proc. of the 1998 ASME/AIAA Wind Energy Symposium*, Reno, pp. 75–83.

[2] "Carbon-Hybrid Blade Developments: With and Without Twist-Coupling," TPI Composites/Global Energy Concepts, Sandia National Laboratories (contractor report to be published).

[3] "Design and Analysis of 9 m Carbon Hybrid Wind Turbine Rotor Blades," Wichita State University/Wetzel Engineering, Inc., Principal Investigator: James Locke, Sandia National Laboratories (contractor report to be published).

[4] Lobitz, D. W., 2004, "Aeroelastic Stability Predictions for a MW-Sized Blade," Wind Energy **7** (3), pp. 211–224.

[5] Hansen, M. H., 2004, "Stability Analysis of Three-Bladed Turbines Using an Eigenvalue Approach," *Proc. of the 2004 ASME/AIAA Wind Energy Symposium*, Reno, pp. 192–202.

[6] Bisplinghoff, R. L., and Ashley, H., 1962, *Principles of Aeroelasticity*, John Wiley and Sons, Inc., New York, Chap. 6.

[7] Dowell, E. E. (Editor), 1995, *A Modern Course in Aeroelasticity*, 3rd ed., Kluwer Academic Publishers, Dordrecht, The Netherlands, Chaps. 3, 4.

[8] Fung, Y. C., 1969, *An Introduction to the Theory of Aeroelasticity*. Dover Publications Inc., New York, Chap. 6.

[9] Bisplinghoff, R. L., Ashley, H., and Halfman, R. L., 1955, *Aeroelasticity*, Addison-Wesley Publishing Company Inc., Menlo Park, CA, Chaps. 1, 5.

[10] Theodorsen, T., 1935, "General Theory of Aerodynamic Instability and the Mechanism of Flutter," NACA, Rept. 496.

[11] MSC Software Corporation, NASTRAN product (www.mscsoftware.com), accessed November 18, 2003.

[12] Malcolm, D. J., and Hansen, A. C., 2002, "WindPACT Rotor Turbine Design Study," National Renewable Energy Laboratory, Rept. NREL/SR-500-32495.

[13] Lobitz, D. W., and Veers, P. S., 2003, "Load Mitigation with Bending/Twist-Coupled Blades on Rotors Using Modern Control Stategies," Wind Energy **6** (2), pp. 105–117.